Chemical Exchange Saturation Transfer (CEST) Imaging

11

Daniel Paech and Lisa Loi

Introduction to Chemical Exchange Saturation Transfer (CEST) Magnetic Resonance Imaging (MRI)

Endogenous low-concentration metabolites or exogenously administered agents, containing either exchangeable protons or molecules, can be imaged using selective radiofrequency (RF) saturation followed by indirect detection via the water signal with large signal amplification [1, 2]. Chemical exchange saturation transfer (CEST) magnetic resonance imaging (MRI) makes use of the spontaneously occurring chemical exchange between solute-bound protons and protons of free bulk water. Magnetization transfer from saturated low-concentration solutes to free water results in a decrease of the water magnetization, which is proportional to the local concentration of the metabolite of interest. Alterations of local tissue properties (e.g., pH changes in ischemic stroke) also affect the proton exchange rates, making CEST MRI additionally sensitive to changes in the microenvironment.

In CEST MRI, successive acquisition of off-resonant saturation at different frequency offsets around the water resonance at $\Delta(\text{Delta})\omega(\text{omega}) = 0$ ppm yields the so-called Z-spectrum (Fig. 11.1),where the intensity of the water signal is plotted as a function of irradiation frequency defining the water frequency as zero-reference [3]. For an adequate pixel-wise determination of the water resonance, it is essential to correct for B_0-field inhomogeneities; e.g., by using the "water saturation shift referencing" or "WASSR" approach [4]. Particularly at ultra-high field strength, additional correction of B_1-field inhomogeneities is crucial for the correct interpretation of CEST data as the effect strength strongly depends on the applied saturation power [5].

Amide proton transfer (APT) imaging is the most frequently studied CEST contrast resonating around $\Delta(\text{Delta})\omega(\text{omega}) = +3.5$ ppm relative to the resonance of free water. This technique has first been applied by Zhou et al. to study pH-alterations caused by ischemic stroke [6]. CEST signal intensities are most commonly quantified by calculating the magnetization transfer ratio asymmetry (MTR_{asym}). This approach is based on the assumption that magnetization transfer effects are symmetric with respect to water resonance. Consequently, e.g., APT CEST effects at $\Delta(\text{Delta})\omega(\text{omega}) = +3.5$ ppm result in a positive magnetization transfer difference, the so-called APT-weighted (APT-w) CEST contrast [6]:

$$\text{MTR}_{\text{asym}}\left(\Delta\omega\right) = \left[\, S_{\text{sat}}\left(-\Delta\omega\right) - S_{\text{sat}}\left(+\Delta\omega\right)\right] / S_0$$

For APT-w CEST imaging based on the MTR_{asym} approach, relatively high RF saturation power (e.g., $B_1 = 2.1$ μ[mu]T) has been reported to maximize the APT effect [7]. In contrast, detection of relayed Nuclear Overhauser Effect (rNOE)-mediated CEST effects, located upfield from the water resonance at approximately at $\Delta(\text{Delta})\omega(\text{omega}) = -2$ to -5 ppm, is improved by using lower saturation power (e.g., $B_1 = 0.6$ μ[mu]T) [8, 9].

Besides the APT effect around +3.5 ppm from water, multiple exchangeable groups (resonating between 1 and 6 ppm from water) may contribute to the MTR_{asym} contrast [2]. In addition, contributions from T_1- and T_2-relaxation [10, 11], conventional semi-solid magnetization transfer (MT) effects [12], and downfield rNOE CEST signals [13] affect the MTR_{asym} metric. Therefore, more sophisticated approaches have been proposed enabling separation of multiple CEST pools, e.g., by using Lorentzian fit analysis on data with sufficiently high spectral resolution (Fig. 11.1) [9, 14, 15].

Direct water proton saturation (spillover) and semi-solid MT effects can be reduced by applying the inverse difference metric introduced by Zaiss et al. in 2013 [16]. Further, correction of T_1-relaxation time can be achieved by using the relaxation-compensated metric, which yields the apparent

D. Paech (✉) · L. Loi
Department of Radiology, German Cancer Research Center, Heidelberg, Germany
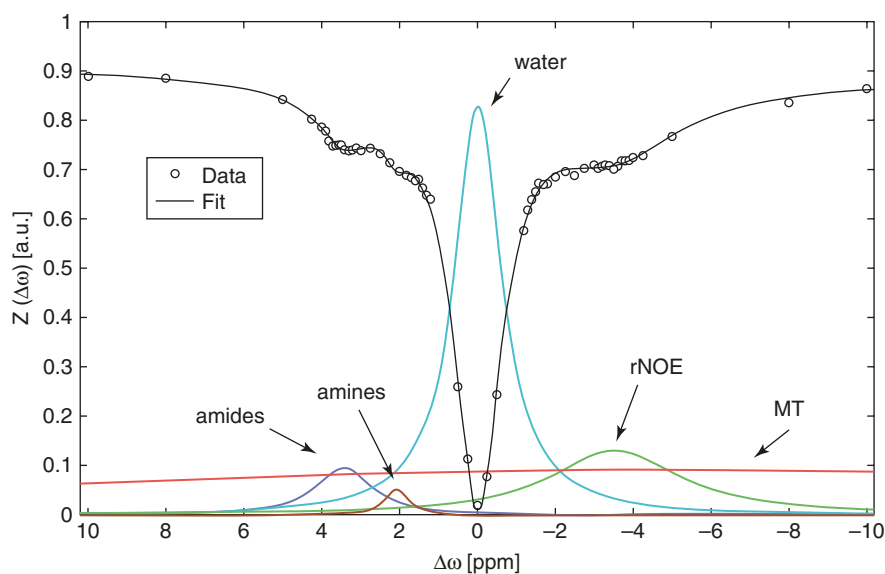e-mail: d.paech@dkfz.de; d.paech@dkfz-heidelberg.de; L.loi@dkfz.de

Fig. 11.1 Z-spectrum acquired in the human brain of a healthy volunteer at 7.0 T. The most prominent resonances at positive frequencies can be assigned to the amide protons (dark blue line) and amines (orange line) resonating around $\Delta\omega = +3.5$ ppm and $\Delta\omega = +2.2$ ppm. A broader resonance can be observed upfield from the water resonance ($\Delta\omega = -2$ ppm to -5 ppm), which is caused by relayed nuclear Overhauser effects (rNOE, green line). The water resonance (per definition at 0 ppm, light blue line) and the very broad semi-solid magnetization transfer (MT, red line) are additionally fitted by Lorentzian functions. *Technical parameters*: Read out: $B_0 = 7$ T, FoV 195×170, matrix 128×112, slice thickness 5 mm, TE = 3.61 ms, TR = 7.4 ms, flip angle 10°. Saturation: 120 Gaussian-shaped pulses à 15 ms; $B_1 = 0.9$ μT; in total 60 offsets

exchange-dependent relaxation rate (AREX) [10, 14, 17–19]. Regarding the last mentioned correction method, it has been shown that T_1-normalization may not be necessary in clinical MRI systems with lower field strength, when appropriate sequence parameters are chosen [20]. Ultimately, downfield resonating rNOE effects can be estimated and reduced yielding the downfield rNOE suppressed (dns-) APT metric [13].

Future prospective large cohort clinical studies need to investigate whether the interfering effects in conventional APT-wMTR$_{asym}$ contrasts add up constructively or if more complex approaches are needed to increase the specificity and the diagnostic value of CEST MRI. Recently, consensus recommendations on clinical APTw imaging approaches have been provided by leading experts in the field to provide a rationale for optimized APTw imaging at 3 T [21].

Neurooncological Applications of CEST MRI

Neurooncological imaging represents one of the major fields of CEST MRI applications. There is a fast growing body of evidence that APT(-w) imaging may add complementary information when included in conventional MRI protocols [22, 23]. CEST MRI approaches have been shown to allow differentiation between different World Health Organization (WHO) tumor grades and molecular tumor subtypes. Furthermore, early therapy response and prognostication have been shown to be associated with protein concentration

alterations detected with CEST MRI. The following sections of this chapter provide an overview of the studies published in the literature (see Table 11.1 for summary of key studies).

Endogenous CEST Contrasts in Neurooncological Applications

In 2003, Zhou et al. described for the first time the application of APT-w CEST MRI in brain tumors [24]. The study was conducted in a rat 9 L gliosarcoma model and showed increased APT signal intensities that were assigned to malignant brain tumor tissue. Since then, APT-w MRI has intensively been investigated, both in animal studies and patients with brain tumors. Increased APT signals in tumors are generally explained by higher concentrations of mobile proteins and peptides in malignant tumors [22, 25, 26]. APT signals have been shown to positively correlate with WHO tumor grade in preoperative imaging of glioma patients [27–30]. In particular, the ability of APT-w CEST MRI to differentiate between high- and low-grade glioma was also reported for non-enhancing lesions [31]. Multiple studies found a positive correlation of APT signals with cell density and proliferation (Ki-67-index) in brain tumors [27, 28, 32–34]. Investigations of CEST MRI at ultra-high field strength (7 T) recently confirmed these findings employing the relaxation-compensated and downfield rNOE suppressed (dns-) APT metric in patients with glioma [35] (Fig. 11.2).

Table 11.1 Summary of key literature

Authors	Article	Summary
Ward, KM et al., 2000	A new class of contrast agents for MRI based on proton chemical exchange dependent saturation transfer (CEST). J Magn Reson. 2000 Mar;143(1):79–87	First article proposing to use exchangeable protons for MRI contrast under physiological conditions and introduced the idea of using exogenous compounds as CEST agents for MRI. In vitro demonstration that selective radiofrequency (RF) saturation enables detection of protons of interest
Zhang et al., 2001	A novel europium (III)-based MRI contrast agent. Journal of the American Chemical Society, 123(7), 1517–1518	The first demonstration of a paramagnetic CEST agent as a MRI agent
Zhou, J et al., 2003	Using the amide proton signals of intracellular proteins and peptides to detect pH effects in MRI. Nature medicine. 2003;9(8):1085–90	First application of pH-sensitive APT CEST imaging for detecting acute stroke in ischemic rat models
Zhou, J et al., 2003	Amide proton transfer (APT) contrast for imaging of brain tumors. Magn Reson Med. 2003 Dec;50(6):1120–6	Initial application of APT CEST MRI in brain tumors (preclinical). Demonstration that APT MRI reflects endogenous cellular protein and peptide content in intracranial rat 9 L gliosarcomas
Van Zijl, PCM et al., 2007	MRI detection of glycogen in vivo by using chemical exchange saturation transfer imaging (glycoCEST). Proceedings of the National Academy of Sciences, 104(11), 4359–4364	In vitro and in vivo detection of glycogen using CEST MRI. Glycogen metabolism could be followed in isolated, perfused mouse livers at 4.7 T before and after administration of glucagon
Sun, PZ et al., 2007	Detection of the ischemic penumbra using pH-weighted MRI. Journal of Cerebral Blood Flow & Metabolism, 27(6), 1129–1136	Twenty-one rats underwent permanent middle cerebral artery occlusion and ischemic evolution over the first 3.5 h post-occlusion was studied using multiparametric MRI. The study showed that pH-weighted CEST MRI provides information complementary to PWI and DWI in the delineation of ischemic tissue
Van Zijl, PCM et al., 2011	Chemical exchange saturation transfer (CEST): what is in a name and what isn't? Magnetic resonance in medicine, 65(4), 927–948	Review article focusing on the basic magnetic resonance principles underlying CEST and similarities to and differences with conventional magnetization transfer contrast. The basic theory, design criteria, and experimental issues for exchange transfer imaging are discussed
Chan, KW et al., 2012	Natural D-glucose as a biodegradable MRI contrast agent for detecting cancer. Magnetic resonance in medicine, 68(6), 1764–1773	Investigation of the possibility of using simple D-glucose as an infusable biodegradable MRI agent for cancer detection in two human breast cancer cell lines, MDA-MB-231 and MCF-7, implanted orthotopically in nude mice
Walker-Samuel, S et al., 2013	In vivo imaging of glucose uptake and metabolism in tumors. Nature medicine, 19(8), 1067–1072	Demonstration that glucose chemical exchange saturation transfer (glucoCEST) is sensitive to tumor glucose accumulation in colorectal tumor models and allows distinguishing tumor types with differing metabolic characteristics and pathophysiologies
Haris M et al., 2013	Imaging of glutamate neurotransmitter alterations in Alzheimer's disease. NMR Biomed. 2013;26(4):386–91	Application of glutamate-sensitive CEST MRI (GluCEST) to detect early stages of Alzheimer's disease in the brain of APP-PS1 transgenic mouse models
Zaiss, M et al., 2013	Chemical exchange saturation transfer (CEST) and MR Z-spectroscopy in vivo: a review of theoretical approaches and methods. Physics in Medicine & Biology, 58(22), R221	Review article considering analytical solutions of the Bloch–McConnell (BM) equation system for the theoretical description of CEST and the equivalent off-resonant spinlock (SL) experiments. Overview of reported CEST effects in vivo and applications on clinical MRI systems
Togao, O et al., 2014	Amide proton transfer imaging of adult diffuse gliomas: correlation with histopathological grades. Neuro-oncology, 16(3), 441–448	The ability of APT imaging to predict the histological grade of adult diffuse gliomas was tested in a cohort of 36 patients with histopathologically proven diffuse glioma
Li C et al., 2014	Chemical exchange saturation transfer MR imaging of Parkinson's disease at 3 Tesla. Eur Radiol. 2014;24(10):2631–9	Feasibility study on the application of CEST MRI to detect Parkinson's disease in 27 patients and 22 healthy controls at 3 T. Region-specific investigation of CEST signals in the substantia nigra and the basal ganglia of Parkinson's disease patients compared to normal controls
Wells JA et al., 2015	In vivo imaging of tau pathology using multi-parametric quantitative MRI. Neuroimage. 2015;111:369–78	Investigation of APT CEST and GlucoCEST MRI in the rTg4510 mouse model of tauopathy to assess neurodegenerative diseases
Davis et al., 2015	Glutamate imaging (GluCEST) lateralizes epileptic foci in nonlesional temporal lobe epilepsy. Sci Transl Med. 2015; 7(309):309ra161.	Glutamate chemical exchange saturation transfer (GluCEST) MRI was applied to patients with non-lesional temporal lobe epilepsy based on conventional MRI and its feasibility to correctly lateralize the temporal lobe seizure focus on glutamate-based images was shown

Table 11.1 (continued)

| Authors	Article	Summary
Zaiss, M et al., 2015	Relaxation-compensated CEST-MRI of the human brain at 7 T: unbiased insight into NOE and amide signal changes in human glioblastoma. Neuroimage, 112, 180–188	Correction algorithm to compensate semi-solid magnetization transfer (MT), as well as T1 scaling and spillover in CEST data yielding the apparent exchange-dependent relaxation (AREX). First application to a study cohort of ten patients with glioblastoma
Xu, X et al., 2015	Dynamic glucose-enhanced (DGE) MRI: translation to human scanning and first results in glioma patients. Tomography, 1(2), 105	Dynamic glucose enhanced (DGE) image data from four normal volunteers and three glioma patients showed a strong signal enhancement in blood vessels, while a spatially varying enhancement was found in brain tumors
Paech, D et al., 2017	T1ρ-weighted dynamic glucose-enhanced MR imaging in the human brain. Radiology, 285(3), 914–922	Adiabatically prepared chemical exchange–sensitive spin-lock imaging at 7.0 T performed in nine patients with glioblastoma and four healthy controls. Pathophysiologically increased glucose concentration in glioblastoma was demonstrated following intravenous administration
O'Grady KP et al., 2019	Glutamate-sensitive imaging and evaluation of cognitive impairment in multiple sclerosis. Mult Scler. 2019 Oct;25(12):1580–1592	Investigation of glutamate-sensitive chemical exchange saturation transfer (GluCEST) MRI in 20 patients with multiple sclerosis revealed increased GluCEST signals in patients with accumulated disability and a positive correlation with symbol digit modality test and choice reaction time scores
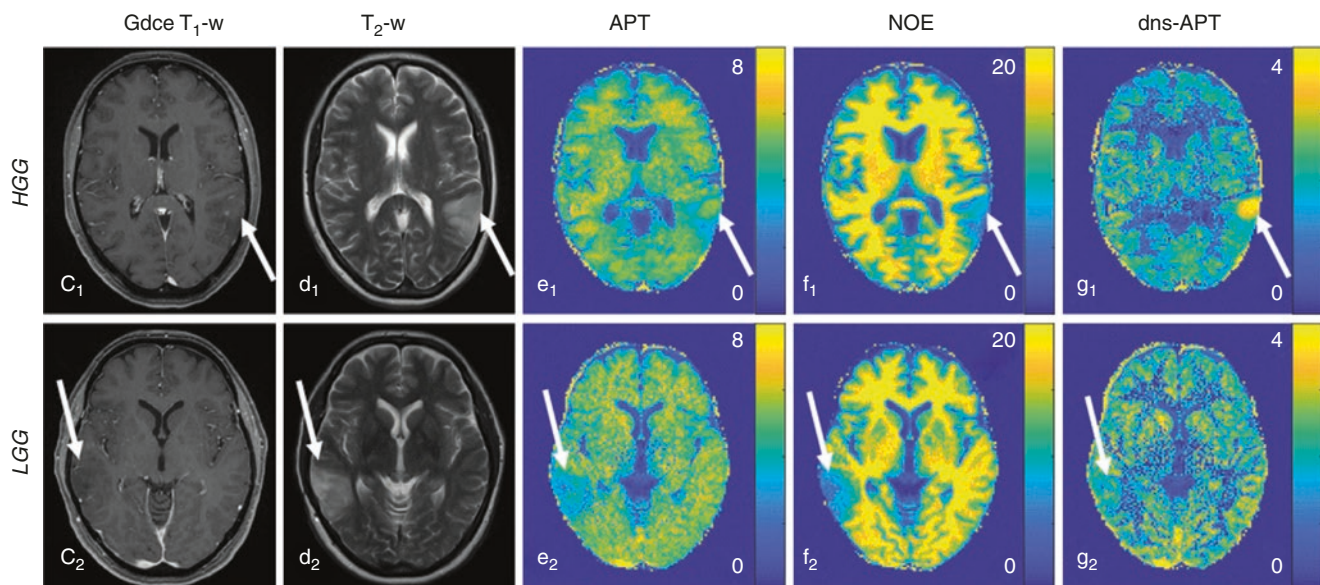
Fig. 11.2 Predictability of World Health Organization (WHO) tumor grade (HGG vs. LGG) in newly diagnosed untreated glioma. Two patients with HGG (GBM, c_1–g_1) and LGG (oligodendroglioma II, c_2–g_2): c_i: GdCE T_1-w, d_i: T_2-w (TSE), relaxation-compensated multipool CEST MRI at 7 T with APT (e_i), NOE (f_i), and dns-APT (g_i) contrasts shown (unit: %). Only a small spot-like contrast enhancement displays in the tumor region of the patient with HGG (c_1), while a clear hyperin- tensity can be observed at dns-APT imaging (g_1, white arrow). (Reproduced with permission from Paech D, Windschuh J, Oberhollenzer J, Dreher C, Sahm F, Meissner JE, et al. Assessing the predictability of IDH mutation and MGMT methylation status in glioma patients using relaxation-compensated multipool CEST MRI at 7.0 T. Neuro Oncol. 2018 Nov 12;20(12):1661–1671)

Another CEST contrast that gained attention in brain tumor imaging is mediated by the relayed nuclear Overhauser enhancement (rNOE)-mediated effect. Decreased rNOE signals are consistently observed in the tumor region of patients with newly diagnosed malignant brain tumors [8, 9, 14]. Further, correlation with tumor grade [36] and cellularity [37] were found for rNOE signals. Thus, both APT(-w) and rNOE imaging may aid more reliable differentiation between tumor and healthy brain tissue.

Assessment of Histopathologic Tumor Subtypes with CEST

Assessment of genetic tumor subtypes such as isocitrate dehydrogenase *(IDH)1* or *IDH2* mutations versus *wild type* forms in patients with glioma are crucial for the therapy planning and prognostication [38]. In clinical routine, invasive procedures such as tumor biopsy or surgical resection are necessary to determine the *IDH* mutation status, as conventional imaging techniques cannot reliably provide this

information. Therefore, intensive efforts are made to develop novel imaging approaches that enable noninvasive determination of the *IDH* mutation status. For instance, magnetic resonance spectroscopy (MRS) has gained considerable attention for the detection of 2-hydroxyglutarate (2-HG) in vivo [39, 40] through its association with the *IDH* mutation status. However, spatial resolution is limited and the acquisition remains challenging, impeding widespread clinical adoption.

Recently, diverse APT CEST MRI approaches have been investigated as alternative noninvasive methods to determine the *IDH*-mutation status in patients with newly diagnosed glioma [35, 41]. These studies found increased APT signals in *IDH* wild-type glioma versus tumors with *IDH* mutation [35, 41]. It is assumed that mutations in *IDH* gene-encoded enzymes cause disturbances of cellular metabolism, including alteration of amino acid concentrations and global down-regulation of protein expression [41]. Supported by the findings of an ultra-high field CEST MRI study, Paech et al. recently suggested that the *IDH* mutation status may have a stronger influence on the APT signal than the WHO tumor grade [35].

Glioma patients with methylated O6-methylguanine-DNA methyltransferase (MGMT) promoter have better outcomes compared to patients with unmethylated MGMT promoter because of the increased chemosensitivity of these tumors [42]. Therefore, MGMT promoter methylation status is another molecular marker of key interest in the diagnostic work-up of glioma patients [35, 43, 44]. Jiang et al. reported significantly decreased APT signals in patients with methylated, compared to unmethylated MGMT promoters [43]. The same trends were also found using the relaxation-compensated APT metric at 7 T; however, statistical significance was not reached [35].

Therapy Response Assessment, Prognostication, and Outcome Prediction with CEST

Early therapy response assessment and prognostication of patients with glioma are major challenges in clinical routine. The updated Response Assessment in Neuro-Oncology (RANO) criteria require repeated post-treatment MRI examinations with gadolinium contrast [45], in order to account for possible pseudo progression early after treatment [45–47].

A preclinical study performed by Zhou et al. in 2011 indicated that APT-w CEST MRI may enable differentiation between tumor recurrence and radiation necrosis in a tumor model of orthotopic glioma (SF188/V+ glioma and 9 L gliosarcoma) in rats [48]. Another animal study demonstrated the ability of APT-w MRI to detect early therapy response-related changes in U87 tumor-bearing rats following radiotherapy [49]. In accordance, APT-w CEST MRI has been shown to be sensitive to early therapy response-induced

changes during treatment with temozolomide in an ortho-topic tumor mouse model of human glioblastoma [50].

In humans, Park et al. found significantly increased APT signals in tumors of patients with progressive glioma compared to tumors of patients with treatment-related changes [51, 52]. APT values were also reported to be moderately correlated with the choline-to-creatine ratio and moderately correlated with the choline-to-*N*-acetylaspartate ratio, obtained with magnetic resonance spectroscopy (MRS) [52].

APT- and rNOE-mediated CEST effects were also shown to allow a differentiation of treatment response from progression in glioma patients immediately after or already during radio-chemotherapy [53, 54]. Furthermore, APT and rNOE CEST imaging enabled pre-treatment discrimination of responders to first-line chemo-radiation therapy versus patients with early progression [53, 55]. Recently, a study found early reduction in mean APT-w CEST signals during antiangiogenic treatment (4–6 weeks after initiation) to be associated with treatment response in patients with recurrent glioma [56]. Consistent with these results, APT CEST signals have additionally been shown to be associated with long-term outcome by means of progression-free survival (PFS) and overall survival in patients with newly diagnosed high-grade glioma (WHO grades III–IV) [57].

Exogenous CEST Contrasts: Glucose-Enhanced MRI of Brain Tumors

The application of contrast agents is of high diagnostic value in neurooncological imaging. MRI contrast agents are generally based on the paramagnetic metal gadolinium (Gd). However, several studies recently reported accumulation of gadolinium in deep gray matter nuclei after serial application of linear gadolinium-based contrast agents (GBCA) [58–63]. Moreover, there is a known risk of developing nephrogenic systemic fibrosis (NSF) for patients with renal failure [64]. Therefore, novel MRI techniques using biodegradable contrast agents are highly desirable. A promising new approach is based on the intravenous administration of natural D-glucose, which can be detected using CEST [65–67] or chemical exchange sensitive spin-lock (CESL) [68, 69]. The principle of these approaches is to measure dynamic signal changes after the intravenous administration of D-glucose (in humans, e.g., 100 mL, concentration: 20% [70]) with high temporal and spatial resolution.

The ability of these approaches to detect increased glucose concentrations in tumors was demonstrated in patients with glioma at 7 T [70–73]. These studies revealed higher glucose concentrations in tumor regions compared to healthy brain tissue [70–73]. Moreover, increased glucose concentrations were also detected in areas beyond the disrupted blood–brain barrier (BBB) (Fig. 11.3).
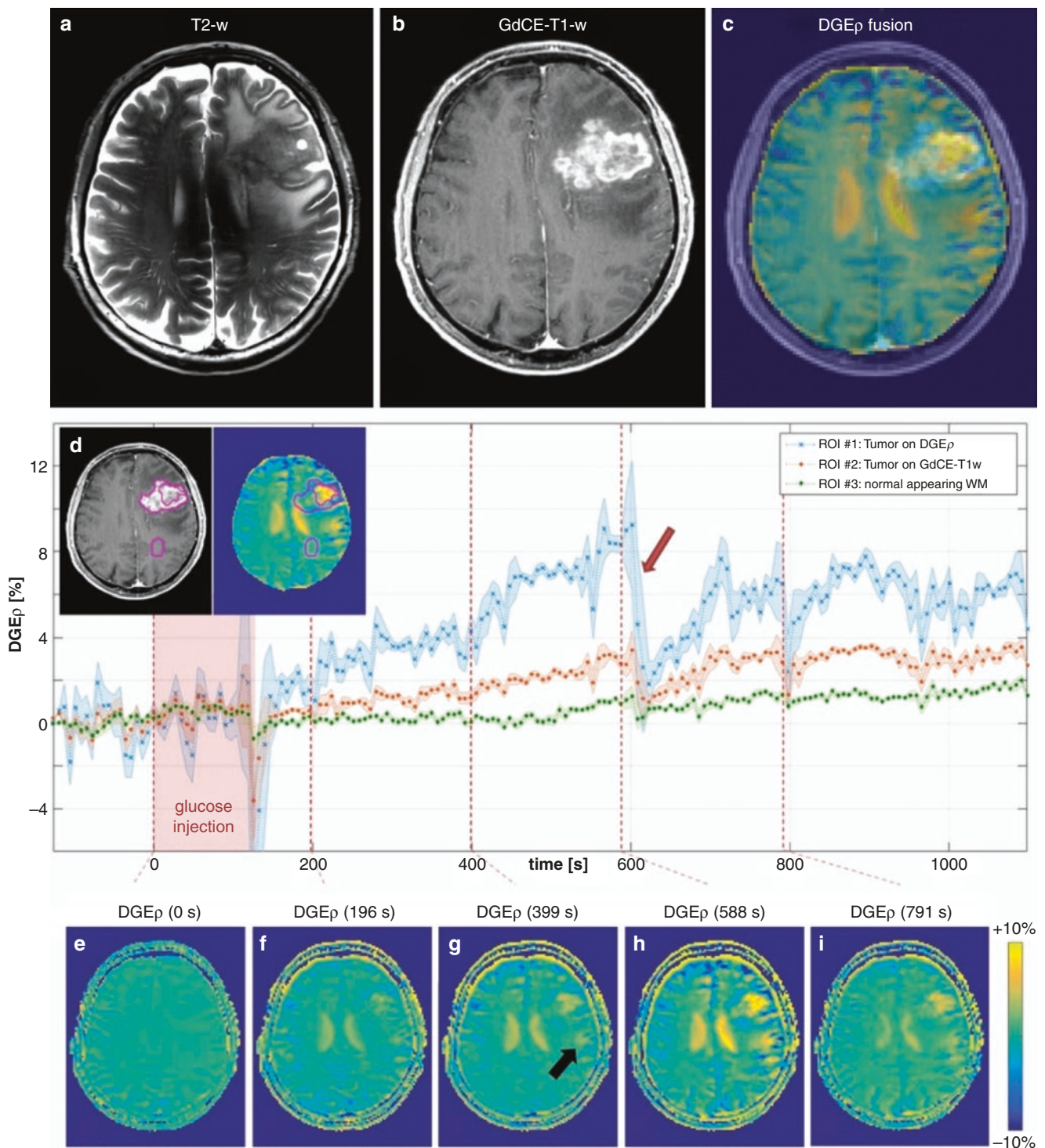
Fig. 11.3 (**a**) T_2-w image acquired at 7 T, (**b**) Gd-enhanced T_1-weighted (GdCE-T1w) image acquired at 3 T, (**c**) fusion of the GdCE-T1w image and the $T_{1\rho}$-weighted dynamic glucose enhancement (DGE_ρ). (**d**) DGE_ρ time curves with a temporal resolution of less than 7 s in a tumor-ROI selected on DGE_ρ (ROI #1), a second tumor-ROI selected on the GdCE-T1w image (ROI #2), and a ROI in normal appearing white matter (ROI #3). Increasing DGE_ρ values are obtained in both tumor-ROIs following glucose injection. The red arrow marks an abrupt signal drop induced by patient motion. (**e–i**) DGE_ρ images (average of 5 consecutive images) at different time points after glucose injection. Note the hyperintense region at the bottom of the tumor area (black arrow; (**g**)), which is not visible in the GdCE-T1w image (**b**). (Figure reprinted under terms of Creative Commons license from Schuenke P, Paech, D, Koehler C, Windschuh J, Bachert P, Ladd ME, et al. Fast and Quantitative T1ρ-weighted Dynamic Glucose Enhanced MRI. *Sci. Rep.* 2017;**7**:42093. http://creativecommons.org/licenses/by/4.0/)

The origin of the signal changes in dynamic glucose-enhanced (DGE) MRI is still under debate. In general, a glucose concentration change in the intravascular space, the extravascular and extracellular space (EES), and the intracellular space can contribute to the signal. The latest results in brain tumor studies suggest that signal changes on DGE-MRI are mainly attributable to BBB leakage and tissue perfusion [70, 72, 74]. Furthermore, both CEST and CESL may be additionally altered by local pH, since an acidic tumor microenvironment can enhance DGE signals through proton exchange rate modulation.

Recently, glucose-enhanced CE-sensitive MRI has also been implemented in glioma patients at clinical field strengths of 3 T employing the CEST [75] and CESL [76] techniques. However, small effect sizes were observed at 3 T compared to previous results at 7 T MRI. Therefore, it is currently in question if a robust DCE imaging approach can be established at field strengths less than 7 T.

pH-Sensitive CEST MRI in Neurooncological Applications

Cancer cells commonly show an altered metabolism and tend to have increased intracellular pH values and decreased extracellular pH values [77, 78]. These changes in the tumor microenvironment particularly result from increased expression and/or upregulated activity of H^+-ATPases [79–82], Na^+-H^+ exchangers [83–85], carbonic anhydrases IX and XII [86, 87], monocarboxylate-H^+ efflux cotransporters of the SLCA16A family [88, 89], and lactate dehydrogenases [90, 91], which lead to an increased transport of protons (H+) and lactate across the cell membrane in the extracellular space. The reversed proton gradient [92, 93] causes an acidification of the extracellular compartment (pHe) and an alkalization of the intracellular space (pHi) with distinct consequences [93–95]. Thus, pH-weighted contrast methods may represent a valuable imaging technique to gain additional insights into various tumor characteristics.

Since the APT exchange rate is known to be base-catalyzed for pH values above ~5 [6, 96, 97], this pH dependence can be used to generate pH-sensitive APT CEST contrasts, first demonstrated by Zhou et al. (2003) in ischemic rat brain models [6]. In contrast to ischemia, tumors show strong alterations of protein and peptide concentrations, which are thought to be the major contributor to the APT-w contrast. Several studies have targeted fast exchanging amine protons (around $\Delta[Delta]\omega[omega] = +3.0$ ppm) in order to obtain in vivo pH maps of tumors [98, 99]. As amide and amine groups of neutral amino acids and glutamine are abundant in active tumor regions [100, 101], Harris et al. [98, 99] demonstrated that a pH-weighted CEST contrast can be obtained in patients with glioma by using amine

CEST. Decreased pHe values were associated with shorter PFS [98]. Consequently, noninvasive windows into pH alterations in tumors provided by novel imaging techniques may have an impact on early identification of malignant transformation in tumors, therapy planning, and prognostication [92, 102].

Assessment of Ischemic and Hemorrhagic Stroke Using CEST MRI

Stroke is a frequent neurological disorder and a leading cause of death and disability in the western countries. There are two main types of brain stroke: ischemic (>80%) and hemorrhagic stroke. For both types, early diagnosis and therapy are crucial. In patients with ischemic stroke, an accurate detection of the ischemic penumbra and an early restoration of sufficient blood flow in these areas are essential to limit the extent of tissue damage. Prior to treatment, imaging by means of computed tomography (CT) (currently main modality) and/or MRI using diffusion-weighed imaging (DWI) and perfusion-weighted imaging (PWI) is decisive in cases of suspected stroke. However, on both CT and conventional MRI, a clear differentiation of ischemic acidosis-based penumbra and benign oligemia remains a challenge in the hyperacute stroke period [103, 104].

pH-Sensitive APT Imaging of Acute Ischemic and Hemorrhagic Stroke

APT-w CEST MRI has been demonstrated to enable a detection of ischemia in acute ischemic stroke patients [105–107]. Insufficiently perfused brain tissue becomes acidotic due to an anaerobic metabolism during early ischemia. Consequently, the base-catalyzed exchange rate of amides and free water protons results in decreasing APT signals. Thus, pH-sensitive APT imaging could be of significant diagnostic value for early stroke imaging, as pH-changes are considered to be one of the first tissue changes during hyperacute ischemic stroke.

Zhou et al. first applied pH-sensitive APT-w CEST imaging to detect acute stroke in ischemic rat brain models. The pH dependence of the APT signal was calibrated in situ, using phosphorus spectroscopy. Comparison of the MTR_{asym} spectrum between ischemic and contralateral regions showed a reduction for the 2–5 ppm offset range [6]. Since then, APT-w CEST MRI has been intensively investigated in different brain ischemic models [108–113]. Sun et al. applied the pH-sensitive APT-w approach in rats after induction of middle cerebral artery occlusion (MCAO) and found a strong correlation of pH-w signal intensity with tissue lactate content by means of ^1H MR spectroscopy [114]. They further

demonstrated that several animals solely showed pH alterations and hypoperfusion on cerebral blood flow (CBF) images, while T_1- and T_2-weighted images were inconspicuous in the hyperacute stage. Moreover, the penumbra detected by pH-sensitive APT-w CEST MRI in the hyperacute period matched very well with the infarcted region on T_2-w images after 24 h [115]. These findings suggest that APT-w CEST MRI may enable early differentiation of ischemic tissue, ischemic acidosis penumbra, and benign oligemia in animal models [116–118].

The translation of pH-based imaging technique to clinical applications yielded similar results: In 2011, Zhao et al. first applied pH-sensitive APT-w CEST MRI to four stroke patients at 3 T and found hypointense APT signals in the infarcted region compared to the normal-appearing brain tissue [119]. Tietze et al. reported significant differences between ischemic brain regions and normal-appearing-white-matter in a study cohort of ten acute stroke patients using pH-sensitive APT-w CEST MRI [106]. More recently, changes of tissue pH were explored in ischemic stroke patients at different phases using APT-w CEST MRI. Depending on the onset time (≤6 h: hyperacute stage, 6–48 h: acute stage, 48–96 h: early subacute stage, 96–168 h:

late subacute stage) patients were assigned to four different groups [105]. APT signals were significantly lower in ischemic tissue over all four stages. Moreover, the results indicated that tissue acidification during stroke decreases as the onset to scan time increases [105]. Generally, all investigations of pH-sensitive APT-w CEST MRI in stroke patients demonstrated the ability of identifying ischemic tissue and that the technique may aid differentiation between ischemic core region, acidosis-based penumbra, and benign oligemia in order to improve initial diagnosis and outcome prediction [105, 107, 119–121] (Fig. 11.4).

Intracerebral Hemorrhage

In preclinical rat models, the comparison of ischemic brain tissue and hyperacute intracerebral hemorrhage revealed opposite APT signal alterations [122]. While ischemic stroke models showed hypointense contrasts, intracerebral hemorrhage appeared hyperintense compared to contralateral healthy brain tissue. The findings were attributed to the accumulation of red and white blood cells, platelets, and protein-rich serums in brain tissue as a consequence of the vessel rupture [122]. This is in line with previous publications describing increased APT signals in blood samples [123].
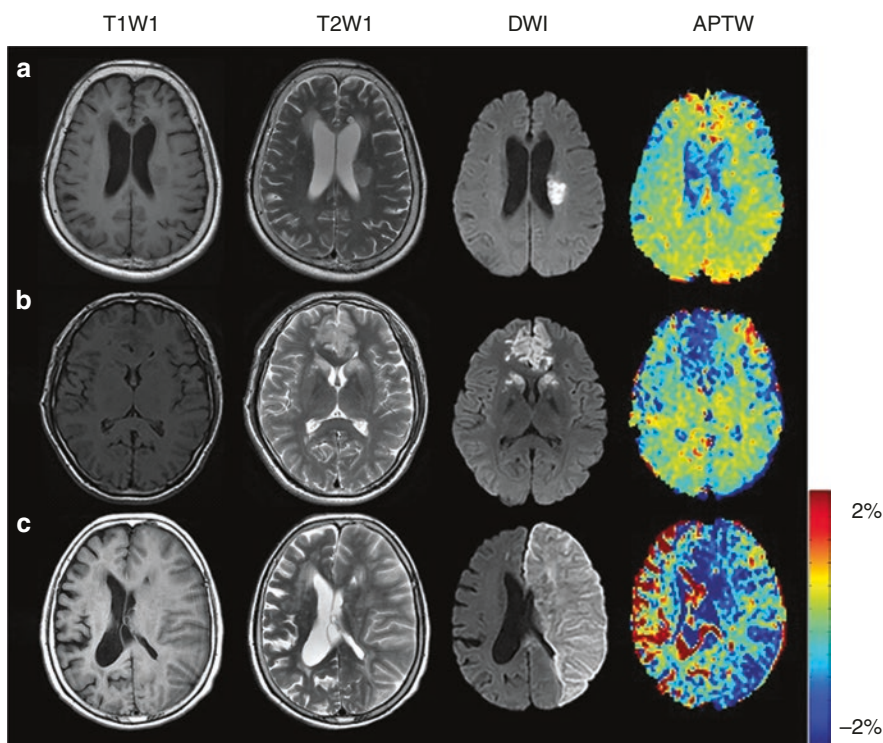

Fig. 11.4 Conventional MR images and APT-w images of patient with acute ischemic stroke of different National Institutes of Health Stroke Scale (NIHSS) scores and 90-day modified Rankin Scale (mRS) scores. Δ(Delta)APTW = Difference of the APT signal between the acute ischemic region and the contralateral side. (**a**) M/65 years, NIHSS score was 3 and 90-day mRS score was 0, Δ(Delta)APTW = −0.37%. (**b**) F/69 years, NIHSS score was 5 and 90-day mRS score was 2, Δ(Delta) APTW = 0.82%. (**c**) M/81 years, NIHSS score was 22 and 90-day mRS score was 6, Δ(Delta)APTW = 1.93%. Areas of acute ischemic stroke display hypointense on APT-w images. (Reprinted under terms of Creative Commons license from Lin G, Zhuang C, Shen Z, Xiao G, Chen Y, Shen Y, Zong X, Wu R. APT Weighted MRI as an Effective Imaging Protocol to Predict Clinical Outcome After Acute Ischemic Stroke. Front. Neurol. 2018;9:901. https://creativecommons.org/licenses/by/4.0/ [121])

The first implementation of APT-w CEST MRI for the early detection of intracerebral hemorrhage in humans was performed by Ma et al. in 2017 [124]. The researchers investigated the APT-w CEST contrast in a study cohort of 33 patients with intracerebral hemorrhage and found significantly increased APT signals in areas of intracerebral hemorrhage at hyperacute, acute, and subacute stages. The authors concluded that APT-wCEST MRI could therefore contribute to noninvasively detect intracerebral hemorrhage at different stages [124].

CEST MRI of Neurodegenerative Diseases

Alzheimer's Disease

Alzheimer's disease (AD) is an irreversible neurological disorder and the major type of dementia in the elderly. In 2019, 46.8 million people worldwide were affected by this age-related disease and AD is gaining increasing importance due to demographic change [125]. Hence, imaging techniques for early AD diagnosis and monitoring of disease progression are desired.

In several AD animal models, APT-wCEST MRI has been studied for targeted detection of AD-associated tau-pathology [126] and amyloid-β(beta) (Aβ[beta]) deposits [127, 128]. As a result, significantly reduced APT-w signals were found in AD models compared to control groups, which was attributed to the effect of protein aggregation during AD [129]. Besides protein aggregation, AD can also be associated with cerebral tissue hypoperfusion and local hypoxia [130] that additionally result in a reduction of the APT signal due to tissue acidification, as previously discussed in detail.

The ability of APT(-w) imaging to detect brain tissue changes in AD patients and to distinguish between different disease stages was first investigated by Wang et al. in 2015 [131]. In contrast to the animal studies described above, significantly increased APT values were found in the hippocampus of AD patients compared to normal controls [131]. This result is consistent with the histological proven accumulation of extracellular amyloid plaques and the appearance of tau proteins into intracellular neurofibrillary tangles that are characteristic for AD [131]. In addition, APT values were negatively correlated with patients' scores in mini-mental state examination (MMSE) [131].

Glutamate-sensitive CEST MRI (GluCEST, Δ[Delta]ω[omega] = 3 ppm) [132] is another CEST contrast that gained attention as a noninvasive biomarker to detect AD at an early stage of disease [133, 134]. Investigations of GluCEST in an APP-PS1 transgenic mouse models of AD showed a reduction of GluCEST signals compared to signals obtained in wild-type controls [133], which is in accordance with studies describing a decrease of glutamate in the early stage of AD [135–137]. Besides glutamate, myoinositol has been demonstrated as a potential molecular target for CEST imaging in preclinical AD mouse models [138, 139]. This metabolite is considered to be associated with amyloid plaque load, microglial activation, and neuroinflammation [139]. Myoinositol-based CEST (MICEST) MRI was firstly investigated by Haris et al. (2011) in healthy humans at ultra-high field strength (7 T) [140]. In addition, the application of MICEST MRI in an APP-PS1 transgenic mouse model of AD revealed about 50% higher MICEST signals in AD mice compared to wild-type controls, which was consistent with the results obtained through proton spectroscopy and immunostaining [138].

Pathological alterations in cerebral D-glucose uptake [141] and 2-deoxy-D-glucose (2DG) uptake [142] in AD mouse models were detected using dynamic glucose-enhanced (DGE) CEST MRI approaches. Recently, on-resonance variable delay multiple pulse (on VDMP) CEST MRI was applied to study D-glucose in a mouse model of AD tauopathy demonstrating its feasibility in discriminating AD mice from wild-type mice [141].

Parkinson's Disease

Parkinson's disease (PD) is a common, gradually progressing neurodegenerative disease characterized by a decreased dopamine level in the dopaminergic neurons in the substantia nigra. Unfortunately, the diagnosis of PD is still based on the clinical manifestations of PD in an advanced stage of the disease. Therefore, novel imaging techniques are required that are sensitive to pathological tissue alterations in the early stages of PD. In this context, a feasibility study of CEST MRI to detect PD showed a decrease of the MTR_{asym} value between the offsets of 0 and 4 ppm in regions of the substantia nigra in comparison with normal controls [143]. Furthermore, a progressive signal intensity decrease from normal controls to early-stage PD and to advanced-stage PD was observed, which is consistent with the increasing loss of dopaminergic neurons in the course of the disease [144, 145]. PD patients with unilateral symptoms showed significantly lower APT-w CEST signal intensities in the substantia nigra on the affected side compared to normal controls [145]. In basal ganglia (e.g., globus pallidus, putamen, and caudate nucleus) of patients with PD, increased APT-w signal intensities were found, which has been speculated to be caused by an accumulation of abnormal cytoplasmic proteins [146].

GluCEST MRI has been investigated in a mouse model of PD and elevated glutamate- signals were observed in the striatum and motor cortex, which positively correlated with MRS-derived glutamate concentrations [147, 148]. Furthermore, a negative correlation between striatal GluCEST signal and motor function was found [148].

Multiple Sclerosis

With a worldwide prevalence of more than 2.2 million patients and a major cause of disability, multiple sclerosis (MS) is a serious neurodegenerative disease of the central nervous system [149]. MS is characterized by a transmigration of immune cells across the blood–brain barrier and a chronic inflammation. Further, demyelination and axonal degeneration in brain tissue and spinal cord represent key features of MS.

In clinical routine, T_1- and T_2-weighted as well as gadolinium (Gd)-enhanced MRI techniques represent the diagnostic gold standard to detect and monitor progression of the disease. However, morphologically visible changes (BBB disruption and contrast enhancement, demyelination, gliosis, and atrophy) are typically related to an advanced stage of MS, so that conventional MRI is insensitive for pathological changes prior to lesion development. For earlier therapeutic intervention and improved prognosis, reliable identification of biochemical changes during the early course of the disease is crucial [150]. In this context, CEST MRI is suggested to aid detecting early tissue changes in patients with MS.

A preclinical study investigated an autoimmune encephalomyelitis (EAE) mouse model prior to the onset of symptoms and found significantly different CEST signals at saturation offsets of 1 and 2 ppm compared to a naïve control group [151]. The expected pathological tissue changes detected by CEST MRI were consistent with follow-up gadolinium-enhanced MRI at the symptom onset and with immunofluorescent staining that was used to confirm the presence of neuroinflammation. Besides early detection of MS, a recent study has shown the potential of on resonance variable delay multiple pulse (on VDMP) CEST MRI to predict disease progression in EAE models of MS [152].

In patients with MS, Dula et al. found a relatively broad APT signal variation in different lesions; an increase in APT-w signal intensity, relative to healthy tissue, was found in some lesions [153]. Applications of GluCEST MRI in patients with relapsing-remitting MS found a trend toward increased GluCEST signals in the cortical GM of MS patients compared to healthy controls and a significant correlation of GluCEST signals with patient performance in a symbol-digit-modality test and choice-reaction time [154]. These results could be explained by a dysfunctional regulation of glutamate in GM, which is expected to be involved in the pathogenesis of MS [155]. As MS affects the entire central nervous system including the spinal cord, CEST MRI was also applied to assess spinal cord lesions in patients with MS [156, 157]. By et al. reported that respiration correction in the spinal cord is necessary to accurately quantify APT values in MS lesions [157]. The respiration-corrected APT approach yielded significant differences between normal-appearing white matter (NAWM) of MS patients and healthy controls; APT values in MS lesions were not significantly different from NAWM in healthy controls [157].

Imaging of Other Neurological Disorders Using Glutamate-Sensitive CEST (GluCEST) MRI

Epilepsy

Epilepsy is a complex neurological disorder and the fourth most common chronic neurological disease after migraines, Alzheimer's disease, and Parkinson's disease [158, 159]. In 60–70% of patients, antiepileptic drugs (AEDs) are effective in suppressing seizures [160]. In patients with drug-resistant epilepsy the identification of epileptogenic brain regions is crucial for a possible neurosurgical resection. Until now, several structural and functional imaging techniques have been applied to localize epileptogenic brain regions, including conventional MRI [161], MRS [162], single-photon emission computed tomography (SPECT) [163], 18-fluoro-deoxyglucose positron emission tomography (18F-FDG-PET) [164], and magnetoencephalography (MEG) [165]. However, currently available imaging methods are often not capable of detecting the seizure focus adequately.

Both preclinical and human studies provide evidence that glutamatergic dysfunction and elevated glutamate levels are involved in neurological disorders such as epilepsy [166, 167]. Thus, GluCEST MRI may provide valuable information on local alterations of tissue glutamate associated with epileptic foci. In 2015, Davis et al. showed the feasibility of GluCEST MRI to correctly lateralize the temporal lobe seizure focus in patients with previously determined non-lesional temporal lobe epilepsy [168]. Furthermore, Neal et al. observed that enhanced peritumoral GluCEST contrasts are associated with recent seizures and drug refractory epilepsy in patients with glioma [169].

Encephalitis

Encephalitis is a central nervous system inflammatory disease that is often caused by viral infections (e.g., herpes simplex viruses) and autoimmune processes [170]. In order to adequately counteract disease progression of infectious and autoimmune encephalitis, early diagnosis is mandatory. Recently, the feasibility of GluCEST imaging for the early diagnosis of encephalitis has been investigated in a preclini-
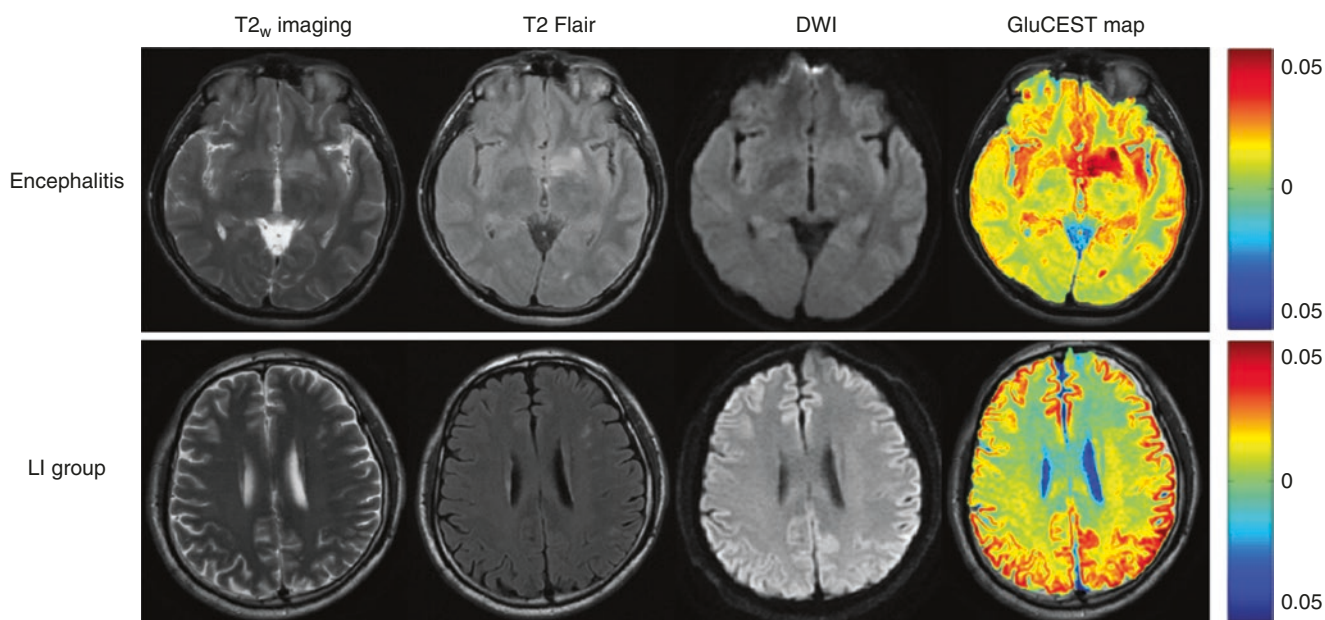
Fig. 11.5 Conventional T_2-w images, T_2-Flair, DWI and GluCEST maps of patients with encephalitis and lacunar infarction (LI). (Reprinted under terms of Creative Commons license from Jia Y, Chen Y, Geng K, Cheng Y, Li Y, Qiu J, Huang H, Wang R, Zhang Y, Wu R. Glutamate Chemical Exchange Saturation Transfer (GluCEST) Magnetic Resonance Imaging in Pre-clinical and Clinical Applications for Encephalitis. *Front. Neurosci.*2020;14:750. https://creativecommons.org/licenses/by/4.0/)

cal and clinical setting [171]. Preclinical research on GluCEST imaging in rats with *Staphylococcus aureus*-induced encephalitis was conducted at 7 T, while clinical investigations were performed at 3 T [172]. Hyperintensities on GluCEST contrasts were observed in the affected areas, both in mouse models and patients with encephalitis [171, 172]. Furthermore, GluCEST MRI has been shown to enable distinguishing between patients with encephalitis and lacunar infarction [171] (Fig. 11.5). In addition, GluCEST signal intensities in patients with encephalitis lesions significantly decreased after intravenous immunoglobulin therapy compared to GluCEST values before treatment [171].

Conclusion

CEST MRI represents a novel imaging technique providing complementary information to conventional MRI protocols. CEST MRI has proven its value in several neuroradiological applications, especially in neurooncology and cerebral ischemia. Furthermore, the application of multiple CEST approaches in various neurodegenerative diseases and brain disorders, such as MS, epilepsy, and encephalitis has shown the potential of CEST MRI as a noninvasive imaging biomarker that could extent the currently available repertoire of functional and metabolic MRI techniques. However, forthcoming prospective studies in larger study cohorts are needed to prove the added clinical value.

References

1. Ward KM, Aletras AH, Balaban RS. A new class of contrast agents for MRI based on proton chemical exchange dependent saturation transfer (CEST). J Magn Reson. 2000;143(1):79–87.
2. van Zijl PCM, Yadav NN. Chemical exchange saturation transfer (CEST): what is in a name and what isn't? Magn Reson Med. 2011;65(4):927–48.
3. Bryant RG. The dynamics of water-protein interactions. Annu Rev Biophys Biomol Struct. 1996;25(1):29–53.
4. Kim M, Gillen J, Landman BA, Zhou J, van Zijl PCM. Water saturation shift referencing (WASSR) for chemical exchange saturation transfer (CEST) experiments. Magn Reson Med. 2009;61(6):1441–50.
5. Windschuh J, Zaiss M, Meissner JE, Paech D, Radbruch A, Ladd ME, et al. Correction of B1-inhomogeneities for relaxation-compensated CEST imaging at 7 T. NMR Biomed. 2015;28(5):529–37.
6. Zhou J, Payen J-F, Wilson DA, Traystman RJ, van Zijl PCM. Using the amide proton signals of intracellular proteins and peptides to detect pH effects in MRI. Nat Med. 2003;9(8):1085–90.
7. Zhou J, Hong X, Zhao X, Gao J-H, Yuan J. APT-weighted and NOE-weighted image contrasts in glioma with different RF saturation powers based on magnetization transfer ratio asymmetry analyses. Magn Reson Med. 2013;70(2):320–7.
8. Paech D, Zaiss M, Meissner J-E, Windschuh J, Wiestler B, Bachert P, et al. Nuclear overhauser enhancement mediated chemical exchange saturation transfer imaging at 7 Tesla in glioblastoma patients. PLoS One. 2014;9(8):e104181.
9. Jones CK, Huang A, Xu J, Edden RA, Schar M, Hua J, et al. Nuclear overhauser enhancement (NOE) imaging in the human brain at 7T. NeuroImage. 2013;77:114–24.
10. Zaiss M, Xu J, Goerke S, Khan IS, Singer RJ, Gore JC, et al. Inverse z-spectrum analysis for spillover-, MT-, and T1-corrected

steady-state pulsed CEST-MRI—application to pH-weighted MRI of acute stroke. NMR Biomed. 2014;27(3):240–52.

11. Moritz Z, Peter B. Chemical exchange saturation transfer (CEST) and MR z-spectroscopy in vivo: a review of theoretical approaches and methods. Phys Med Biol. 2013;58(22):R221.

12. Zaiss M, Zu Z, Xu J, Schuenke P, Gochberg DF, Gore JC, et al. A combined analytical solution for chemical exchange saturation transfer and semi-solid magnetization transfer. NMR Biomed. 2015;28(2):217–30.

13. Zaiss M, Windschuh J, Goerke S, Paech D, Meissner J-E, Burth S, et al. Downfield-NOE-suppressed amide-CEST-MRI at 7 Tesla provides a unique contrast in human glioblastoma. Magn Reson Med. 2017;77(1):196–208.

14. Zaiss M, Windschuh J, Paech D, Meissner J-E, Burth S, Schmitt B, et al. Relaxation-compensated CEST-MRI of the human brain at 7 T: unbiased insight into NOE and amide signal changes in human glioblastoma. NeuroImage. 2015;112:180–8.

15. Zaiß M, Schmitt B, Bachert P. Quantitative separation of CEST effect from magnetization transfer and spillover effects by Lorentzian-line-fit analysis of z-spectra. J Magn Reson. 2011;211(2):149–55.

16. Zaiss M, Bachert P. Exchange-dependent relaxation in the rotating frame for slow and intermediate exchange—modeling off-resonant spin-lock and chemical exchange saturation transfer. NMR Biomed. 2013;26(5):507–18.

17. Zaiss M, Bachert P. Chemical exchange saturation transfer (CEST) and MRZ-spectroscopy in vivo: a review of theoretical approaches and methods. Phys Med Biol. 2013;58(22):R221–R69.

18. Zimmermann F, Korzowski A, Breitling J, Meissner JE, Schuenke P, Loi L, et al. A novel normalization for amide proton transfer CEST MRI to correct for fat signal-induced artifacts: application to human breast cancer imaging. Magn Reson Med. 2020;83(3):920–34.

19. Loi L, Zimmermann F, Goerke S, Korzowski A, Meissner JE, Deike-Hofmann K, et al. Relaxation-compensated CEST (chemical exchange saturation transfer) imaging in breast cancer diagnostics at 7T. Eur J Radiol. 2020;129:109068.

20. Zu Z. Towards the complex dependence of MTR_{asym} on T_{1w} in amide proton transfer (APT) imaging. NMR Biomed. 2018;31(7):e3934.

21. Zhou J, Zaiss M, Knutsson L, Sun PZ, Ahn SS, Aime S, et al. Review and consensus recommendations on clinical APT-weighted imaging approaches at 3T: application to brain tumors. Magn Reson Med. 2022;88(2):546–74. https://pubmed.ncbi.nlm.nih.gov/35452155/. https://doi.org/10.1002/mrm.29241.

22. Wen Z, Hu S, Huang F, Wang X, Guo L, Quan X, et al. MR imaging of high-grade brain tumors using endogenous protein and peptide-based contrast. NeuroImage. 2010;51(2):616–22.

23. Goerke S, Soehngen Y, Deshmane A, Zaiss M, Breitling J, Boyd PS, et al. Relaxation-compensated APT and rNOE CEST-MRI of human brain tumors at 3 T. Magn Reson Med. 2019;82(2):622–32.

24. Zhou J, Lal B, Wilson DA, Laterra J, van Zijl PCM. Amide proton transfer (APT) contrast for imaging of brain tumors. Magn Reson Med. 2003;50(6):1120–6.

25. Jones CK, Schlosser MJ, van Zijl PCM, Pomper MG, Golay X, Zhou J. Amide proton transfer imaging of human brain tumors at 3T. Magn Reson Med. 2006;56(3):585–92.

26. Yan K, Fu Z, Yang C, Zhang K, Jiang S, Lee D-H, et al. Assessing amide proton transfer (APT) MRI contrast origins in 9 L gliosarcoma in the rat brain using proteomic analysis. Mol Imaging Biol. 2015;17(4):479–87.

27. Togao O, Yoshiura T, Keupp J, Hiwatashi A, Yamashita K, Kikuchi K, et al. Amide proton transfer imaging of adult diffuse gliomas: correlation with histopathological grades. Neuro-Oncology. 2014;16(3):441–8.

28. Bai Y, Lin Y, Zhang W, Kong L, Wang L, Zuo P, et al. Noninvasive amide proton transfer magnetic resonance imaging in evaluating the grading and cellularity of gliomas. Oncotarget. 2017;8(4):5834–42.

29. Sakata A, Okada T, Yamamoto A, Kanagaki M, Fushimi Y, Okada T, et al. Grading glial tumors with amide proton transfer MR imaging: different analytical approaches. J Neuro-Oncol. 2015;122(2):339–48.

30. Choi YS, Ahn SS, Lee S-K, Chang JH, Kang S-G, Kim SH, et al. Amide proton transfer imaging to discriminate between low- and high-grade gliomas: added value to apparent diffusion coefficient and relative cerebral blood volume. Eur Radiol. 2017;27(8):3181–9.

31. Togao O, Hiwatashi A, Yamashita K, Kikuchi K, Keupp J, Yoshimoto K, et al. Grading diffuse gliomas without intense contrast enhancement by amide proton transfer MR imaging: comparisons with diffusion- and perfusion-weighted imaging. Eur Radiol. 2017;27(2):578–88.

32. Su C, Liu C, Zhao L, Jiang J, Zhang J, Li S, et al. Amide proton transfer imaging allows detection of glioma grades and tumor proliferation: comparison with Ki-67 expression and proton MR spectroscopy imaging. Am J Neuroradiol. 2017;38(9):1702–9.

33. Jiang S, Eberhart CG, Zhang Y, Heo H-Y, Wen Z, Blair L, et al. Amide proton transfer-weighted magnetic resonance image-guided stereotactic biopsy in patients with newly diagnosed gliomas. Eur J Cancer. 2017;83:9–18.

34. Dreher C, Oberhollenzer J, Meissner J-E, Windschuh J, Schuenke P, Regnery S, et al. Chemical exchange saturation transfer (CEST) signal intensity at 7T MRI of WHO IV° gliomas is dependent on the anatomic location. J Magn Reson Imaging. 2019;49(3):777–85.

35. Paech D, Windschuh J, Oberhollenzer J, Dreher C, Sahm F, Meissner J-E, et al. Assessing the predictability of IDH mutation and MGMT methylation status in glioma patients using relaxation-compensated multi-pool CEST MRI at 7.0 Tesla. Neuro-Oncology. 2018;20(12):1661–71.

36. Heo H-Y, Jones CK, Hua J, Yadav N, Agarwal S, Zhou J, et al. Whole-brain amide proton transfer (APT) and nuclear overhauser enhancement (NOE) imaging in glioma patients using low-power steady-state pulsed chemical exchange saturation transfer (CEST) imaging at 7T. J Magn Reson Imaging. 2016;44(1):41–50.

37. Paech D, Burth S, Windschuh J, Meissner J-E, Zaiss M, Eidel O, et al. Nuclear overhauser enhancement imaging of glioblastoma at 7 Tesla: region specific correlation with apparent diffusion coefficient and histology. PLoS One. 2015;10(3):e0121220.

38. Yan H, Parsons DW, Jin G, McLendon R, Rasheed BA, Yuan W, et al. IDH_1 and IDH_2 mutations in gliomas. N Engl J Med. 2009;360(8):765–73.

39. Choi C, Ganji SK, DeBerardinis RJ, Hatanpaa KJ, Rakheja D, Kovacs Z, et al. 2-Hydroxyglutarate detection by magnetic resonance spectroscopy in IDH-mutated patients with gliomas. Nat Med. 2012;18:624.

40. Pope WB, Prins RM, Albert Thomas M, Nagarajan R, Yen KE, Bittinger MA, et al. Non-invasive detection of 2-hydroxyglutarate and other metabolites in IDH_1 mutant glioma patients using magnetic resonance spectroscopy. J Neuro-Oncol. 2012;107(1):197–205.

41. Jiang S, Zou T, Eberhart CG, Villalobos MAV, Heo HY, Zhang Y, et al. Predicting IDH mutation status in grade II gliomas using amide proton transfer-weighted (APT_W) MRI. Magn Reson Med. 2017;78(3):1100–9.

42. Hegi ME, Diserens A-C, Gorlia T, Hamou M-F, de Tribolet N, Weller M, et al. MGMT gene silencing and benefit from temozolomide in glioblastoma. N Engl J Med. 2005;352(10):997–1003.

43. Jiang S, Rui Q, Wang Y, Heo H-Y, Zou T, Yu H, et al. Discriminating MGMT promoter methylation status in patients with glioblastoma

employing amide proton transfer-weighted MRI metrics. Eur Radiol. 2018;28(5):2115–23.

44. Oue N, Shigeishi H, Kuniyasu H, Yokozaki H, Kuraoka K, Ito R, et al. Promoter hypermethylation of MGMT is associated with protein loss in gastric carcinoma. Int J Cancer. 2001;93(6):805–9.

45. Wen PY, Macdonald DR, Reardon DA, Cloughesy TF, Sorensen AG, Galanis E, et al. Updated response assessment criteria for high-grade gliomas: response assessment in neuro-oncology working group. J Clin Oncol. 2010;28(11):1963–72.

46. Brandsma D, Stalpers L, Taal W, Sminia P, van den Bent MJ. Clinical features, mechanisms, and management of pseudoprogression in malignant gliomas. Lancet Oncol. 2008;9(5):453–61.

47. de Wit MC, de Bruin HG, Eijkenboom W, Sillevis Smitt PA, van den Bent MJ. Immediate post-radiotherapy changes in malignant glioma can mimic tumor progression. Neurology. 2004;63(3):535–7.

48. Zhou J, Tryggestad E, Wen Z, Lal B, Zhou T, Grossman R, et al. Differentiation between glioma and radiation necrosis using molecular magnetic resonance imaging of endogenous proteins and peptides. Nat Med. 2011;17(1):130–4.

49. Hong X, Liu L, Wang M, Ding K, Fan Y, Ma B, et al. Quantitative multiparametric MRI assessment of glioma response to radiotherapy in a rat model. Neuro-Oncology. 2014;16(6):856–67.

50. Sagiyama K, Mashimo T, Togao O, Vemireddy V, Hatanpaa KJ, Maher EA, et al. In vivo chemical exchange saturation transfer imaging allows early detection of a therapeutic response in glioblastoma. Proc Natl Acad Sci U S A. 2014;111(12):4542–7.

51. Park KJ, Kim HS, Park JE, Shim WH, Kim SJ, Smith SA. Added value of amide proton transfer imaging to conventional and perfusion MR imaging for evaluating the treatment response of newly diagnosed glioblastoma. Eur Radiol. 2016;26(12):4390–403.

52. Park JE, Kim HS, Park KJ, Kim SJ, Kim JH, Smith SA. Pre- and posttreatment glioma: comparison of amide proton transfer imaging with MR spectroscopy for biomarkers of tumor proliferation. Radiology. 2016;278(2):514–23.

53. Mehrabian H, Myrehaug S, Soliman H, Sahgal A, Stanisz GJ. Evaluation of glioblastoma response to therapy with chemical exchange saturation transfer. Int J Radiat Oncol Biol Phys. 2018;101(3):713–23.

54. Meissner J-E, Korzowski A, Regnery S, Goerke S, Breitling J, Floca RO, et al. Early response assessment of glioma patients to definitive chemoradiotherapy using chemical exchange saturation transfer imaging at 7 T. J Magn Reson Imaging. 2019;50(4):1268–77.

55. Regnery S, Adeberg S, Dreher C, Oberhollenzer J, Meissner J-E, Goerke S, et al. Chemical exchange saturation transfer MRI serves as predictor of early progression in glioblastoma patients. Oncotarget. 2018;9(47):28772–83.

56. Park JE, Kim HS, Park SY, Jung SC, Kim JH, Heo HY. Identification of early response to anti-angiogenic therapy in recurrent glioblastoma: amide proton transfer-weighted and perfusion-weighted MRI compared with diffusion-weighted MRI. Radiology. 2020;295(2):397–406.

57. Paech D, Dreher C, Regnery S, Meissner J-E, Goerke S, Windschuh J, et al. Relaxation-compensated amide proton transfer (APT) MRI signal intensity is associated with survival and progression in high-grade glioma patients. Eur Radiol. 2019;29(9):4957–67.

58. Radbruch A, Weberling LD, Kieslich PJ, Eidel O, Burth S, Kickingereder P, et al. Gadolinium retention in the dentate nucleus and globus pallidus is dependent on the class of contrast agent. Radiology. 2015;275(3):783–91.

59. Kanda T, Ishii K, Kawaguchi H, Kitajima K, Takenaka D. High signal intensity in the dentate nucleus and globus pallidus on unenhanced T1-weighted MR images: relationship with increasing cumulative dose of a gadolinium-based contrast material. Radiology. 2014;270(3):834–41.

60. Kanda T, Osawa M, Oba H, Toyoda K, Kotoku J, Haruyama T, et al. High signal intensity in dentate nucleus on unenhanced T1-weighted MR images: association with linear versus macrocyclic gadolinium chelate administration. Radiology. 2015;275(3):803–9.

61. McDonald RJ, McDonald JS, Kallmes DF, Jentoft ME, Murray DL, Thielen KR, et al. Intracranial gadolinium deposition after contrast-enhanced MR imaging. Radiology. 2015;275(3):772–82.

62. Radbruch A, Haase R, Kickingereder P, Bäumer P, Bickelhaupt S, Paech D, et al. Pediatric brain: no increased signal intensity in the dentate nucleus on unenhanced T1-weighted MR images after consecutive exposure to a macrocyclic gadolinium-based contrast agent. Radiology. 2017;283(3):828–36.

63. Radbruch A. Are some agents less likely to deposit gadolinium in the brain? Magn Reson Imaging. 2016;34(10):1351–4.

64. Thomsen HS, Morcos SK, Almén T, Bellin M-F, Bertolotto M, Bongartz G, et al. Nephrogenic systemic fibrosis and gadolinium-based contrast media: updated ESUR contrast medium safety committee guidelines. Eur Radiol. 2012;23(2):307–18.

65. Chan KWY, McMahon MT, Kato Y, Liu G, Bulte JWM, Bhujwalla ZM, et al. Natural D-glucose as a biodegradable MRI contrast agent for detecting cancer. Magn Reson Med. 2012;68(6):1764–73.

66. Rivlin M, Horev J, Tsarfaty I, Navon G. Molecular imaging of tumors and metastases using chemical exchange saturation transfer (CEST) MRI. Sci Rep. 2013;3.

67. Walker-Samuel S, Ramasawmy R, Torrealdea F, Rega M, Rajkumar V, Johnson SP, et al. In vivo imaging of glucose uptake and metabolism in tumors. Nat Med. 2013;19(8):1067–72.

68. Jin T, Mehrens H, Hendrich KS, Kim S-G. Mapping brain glucose uptake with chemical exchange-sensitive spin-lock magnetic resonance imaging. J Cereb Blood Flow Metab. 2014;34(8):1402–10.

69. Schuenke P, Koehler C, Korzowski A, Windschuh J, Bachert P, Ladd ME, et al. Adiabatically prepared spin-lock approach for T1ρ-based dynamic glucose enhanced MRI at ultrahigh fields. Magn Reson Med. 2017;78(1):215–25.

70. Paech D, Schuenke P, Koehler C, Windschuh J, Mundiyanapurath S, Bickelhaupt S, et al. T1ρ-weighted dynamic glucose-enhanced MR imaging in the human brain. Radiology. 2017;285(3):914–22.

71. Schuenke P, Paech D, Koehler C, Windschuh J, Bachert P, Ladd M, et al. Fast and quantitative T1ρ-weighted dynamic glucose enhanced MRI. Sci Rep. 2017;7:42093.

72. Xu X, Yadav NN, Knutsson L, Hua J, Kalyani R, Hall E, et al. Dynamic glucose-enhanced (DGE) MRI: translation to human scanning and first results in glioma patients. Tomography. 2015;1(2):105.

73. Boyd PS, Breitling J, Zimmermann F, Korzowski A, Zaiss M, Schuenke P, et al. Dynamic glucose-enhanced (DGE) MRI in the human brain at 7 T with reduced motion-induced artifacts based on quantitative R1ρ mapping. Magn Reson Med. 2020;84(1):182–91.

74. Tao J, Bistra I, Kevin HT, Michel M, Ping W, Hunter M, et al. Chemical exchange–sensitive spin-lock (CESL) MRI of glucose and analogs in brain tumors. Magn Reson Med. 2018;80(2):488–95.

75. Xu X, Sehgal AA, Yadav NN, Laterra J, Blair L, Blakeley J, et al. D-glucose weighted chemical exchange saturation transfer (glucoCEST)-based dynamic glucose enhanced (DGE) MRI at 3T: early experience in healthy volunteers and brain tumor patients. Magn Reson Med. 2020;84(1):247–62.

76. Herz K, Lindig T, Deshmane A, Schittenhelm J, Skardelly M, Bender B, et al. T1ρ-based dynamic glucose-enhanced (DGEP) MRI at 3 T: method development and early clinical experience in the human brain. Magn Reson Med. 2019;82(5):1832–47.

77. Gatenby RA, Gillies RJ. Why do cancers have high aerobic glycolysis? Nat Rev Cancer. 2004;4(11):891–9.

78. Korzowski A, Weinfurtner N, Mueller S, Breitling J, Goerke S, Schlemmer H-P, et al. Volumetric mapping of intra- and extracel-

lular pH in the human brain using 31P MRSI at 7T. Magn Reson Med. 2020;84(4):1707–23.

79. Martinez-Zaguilan R, Lynch RM, Martinez GM, Gillies RJ. Vacuolar-type H (+)-ATPases are functionally expressed in plasma membranes of human tumor cells. Am J Phys Cell Phys. 1993;265(4):C1015–C29.

80. Sennoune SR, Bakunts K, Martínez GM, Chua-Tuan JL, Kebir Y, Attaya MN, et al. Vacuolar H+-ATPase in human breast cancer cells with distinct metastatic potential: distribution and functional activity. Am J Phys Cell Phys. 2004;286(6):C1443–C52.

81. Harguindey S, Orive G, Pedraz JL, Paradiso A, Reshkin SJ. The role of pH dynamics and the Na+/H+ antiporter in the etiopathogenesis and treatment of cancer. Two faces of the same coin—one single nature. Biochim Biophys Acta. 2005;1756(1):1–24.

82. Di Cristofori A, Ferrero S, Bertolini I, Gaudioso G, Russo MV, Berno V, et al. The vacuolar H+ ATPase is a novel therapeutic target for glioblastoma. Oncotarget. 2015;6(19):17514.

83. Miraglia E, Viarisio D, Riganti C, Costamagna C, Ghigo D, Bosia A. Na+/H+ exchanger activity is increased in doxorubicin-resistant human colon cancer cells and its modulation modifies the sensitivity of the cells to doxorubicin. Int J Cancer. 2005;115(6):924–9.

84. Chiang Y, Chou CY, Hsu KF, Huang YF, Shen MR. EGF upregulates Na+/H+ exchanger NHE1 by post-translational regulation that is important for cervical cancer cell invasiveness. J Cell Physiol. 2008;214(3):810–9.

85. Cong D, Zhu W, Shi Y, Pointer KB, Clark PA, Shen H, et al. Upregulation of NHE1 protein expression enables glioblastoma cells to escape TMZ-mediated toxicity via increased H+ extrusion, cell migration and survival. Carcinogenesis. 2014;35(9):2014–24.

86. Chiche J, Ilc K, Laferrière J, Trottier E, Dayan F, Mazure NM, et al. Hypoxia-inducible carbonic anhydrase IX and XII promote tumor cell growth by counteracting acidosis through the regulation of the intracellular pH. Cancer Res. 2009;69(1):358–68.

87. Swietach Á, Hulikova A, Vaughan-Jones R, Harris A. New insights into the physiological role of carbonic anhydrase IX in tumour pH regulation. Oncogene. 2010;29(50):6509.

88. Miranda-Goncalves V, Honavar M, Pinheiro C, Martinho O, Pires MM, Pinheiro C, et al. Monocarboxylate transporters (MCTS) in gliomas: expression and exploitation as therapeutic targets. Neuro-Oncology. 2012;15(2):172–88.

89. Pinheiro C, Reis RM, Ricardo S, Longatto-Filho A, Schmitt F, Baltazar F. Expression of monocarboxylate transporters 1, 2, and 4 in human tumours and their association with CD147 and CD44. Biomed Res Int. 2010;2010:427694.

90. Fantin VR, St-Pierre J, Leder P. Attenuation of LDH-A expression uncovers a link between glycolysis, mitochondrial physiology, and tumor maintenance. Cancer Cell. 2006;9(6):425–34.

91. DeBrosse C, Nanga RPR, Bagga P, Nath K, Haris M, Marincola F, et al. Lactate chemical exchange saturation transfer (LATEST) imaging in vivo: a biomarker for LDH activity. Sci Rep. 2016;6:19517.

92. Wenger KJ, Hattingen E, Franz K, Steinbach JP, Bähr O, Pilatus U. Intracellular pH measured by 31P-MR-spectroscopy might predict site of progression in recurrent glioblastoma under antiangiogenic therapy. J Magn Reson Imaging. 2017;46(4):1200–8.

93. Fais S, Venturi G, Gatenby B. Microenvironmental acidosis in carcinogenesis and metastases: new strategies in prevention and therapy. Cancer Metastasis Rev. 2014;33(4):1095–108.

94. Huber V, De Milito A, Harguindey S, Reshkin SJ, Wahl ML, Rauch C, et al. Proton dynamics in cancer. J Transl Med. 2010;8(1):57.

95. Webb BA, Chimenti M, Jacobson MP, Barber DL. Dysregulated pH: a perfect storm for cancer progression. Nat Rev Cancer. 2011;11:671.

96. Sun PZ, Benner T, Copen WA, Sorensen AG. Early experience of translating pH-weighted MRI to image human subjects at 3 Tesla. Stroke. 2010;41(10_suppl_1):S147–51.

97. Bodet O, Goerke S, Behl NG, Roeloffs V, Zaiss M, Bachert P. Amide proton transfer of carnosine in aqueous solution studied in vitro by WEX and CEST experiments. NMR Biomed. 2015;28(9):1097–103.

98. Harris RJ, Cloughesy TF, Liau LM, Prins RM, Antonios JP, Li D, et al. pH-weighted molecular imaging of gliomas using amine chemical exchange saturation transfer MRI. Neuro-Oncology. 2015;17(11):1514–24.

99. Harris RJ, Cloughesy TF, Liau LM, Nghiemphu PL, Lai A, Pope WB, et al. Simulation, phantom validation, and clinical evaluation of fast pH-weighted molecular imaging using amine chemical exchange saturation transfer echo planar imaging (CEST-EPI) in glioma at 3 T. NMR Biomed. 2016;29(11):1563–76.

100. Souba WW. Glutamine and cancer. Ann Surg. 1993;218(6):715–28.

101. Kovačević Z, Morris HP. The role of glutamine in the oxidative metabolism of malignant cells. Cancer Res. 1972;32(2):326–33.

102. Maintz D, Heindel W, Kugel H, Jaeger R, Lackner KJ. Phosphorus-31 MR spectroscopy of normal adult human brain and brain tumours. NMR Biomed. 2002;15(1):18–27.

103. Fiehler J, Foth M, Kucinski T, Knab R, von Bezold M, Weiller C, et al. Severe ADC decreases do not predict irreversible tissue damage in humans. Stroke. 2002;33(1):79–86.

104. Rivers CS, Wardlaw JM, Armitage PA, Bastin ME, Carpenter TK, Cvoro V, et al. Do acute diffusion- and perfusion-weighted MRI lesions identify final infarct volume in ischemic stroke? Stroke. 2006;37(1):98–104.

105. Song G, Li C, Luo X, Zhao X, Zhang S, Zhang Y, et al. Evolution of cerebral ischemia assessed by amide proton transfer-weighted MRI. Front Neurol. 2017;8:67.

106. Tietze A, Blicher J, Mikkelsen IK, Ostergaard L, Strother MK, Smith SA, et al. Assessment of ischemic penumbra in patients with hyperacute stroke using amide proton transfer (APT) chemical exchange saturation transfer (CEST) MRI. NMR Biomed. 2014;27(2):163–74.

107. Harston GW, Tee YK, Blockley N, Okell TW, Thandeswaran S, Shaya G, et al. Identifying the ischaemic penumbra using pH-weighted magnetic resonance imaging. Brain. 2015;138(Pt 1):36–42.

108. Wu Y, Zhou IY, Lu D, Manderville E, Lo EH, Zheng H, et al. pH-sensitive amide proton transfer effect dominates the magnetization transfer asymmetry contrast during acute ischemia-quantification of multipool contribution to in vivo CEST MRI. Magn Reson Med. 2018;79(3):1602–8.

109. Jin T, Wang P, Hitchens TK, Kim SG. Enhancing sensitivity of pH-weighted MRI with combination of amide and guanidyl CEST. NeuroImage. 2017;157:341–50.

110. Wu L, Jiang L, Sun PZ. Investigating the origin of pH-sensitive magnetization transfer ratio asymmetry MRI contrast during the acute stroke: correction of t(1) change reveals the dominant amide proton transfer MRI signal. Magn Reson Med. 2020;84(5):2702–12.

111. Sun PZ, Wang E, Cheung JS. Imaging acute ischemic tissue acidosis with pH-sensitive endogenous amide proton transfer (APT) MRI—correction of tissue relaxation and concomitant RF irradiation effects toward mapping quantitative cerebral tissue pH. Neuroimage. 2012;60(1):1–6.

112. Zong X, Wang P, Kim SG, Jin T. Sensitivity and source of amine-proton exchange and amide-proton transfer magnetic resonance imaging in cerebral ischemia. Magn Reson Med. 2014;71(1):118–32.

113. Jokivarsi KT, Gröhn HI, Gröhn OH, Kauppinen RA. Proton transfer ratio, lactate, and intracellular pH in acute cerebral ischemia. Magn Reson Med. 2007;57(4):647–53.

114. Sun PZ, Cheung JS, Wang E, Lo EH. Association between pH-weighted endogenous amide proton chemical exchange satura-

tion transfer MRI and tissue lactic acidosis during acute ischemic stroke. J Cereb Blood Flow Metab. 2011;31(8):1743–50.

115. Sun PZ, Zhou J, Sun W, Huang J, van Zijl PC. Detection of the ischemic penumbra using pH-weighted MRI. J Cereb Blood Flow Metab. 2007;27(6):1129–36.

116. Zhou J, van Zijl PC. Defining an acidosis-based ischemic penumbra from pH-weighted MRI. Transl Stroke Res. 2011;3(1):76–83.

117. Guo Y, Zhou IY, Chan ST, Wang Y, Mandeville ET, Igarashi T, et al. pH-sensitive MRI demarcates graded tissue acidification during acute stroke—pH specificity enhancement with magnetization transfer and relaxation-normalized amide proton transfer (APT) MRI. NeuroImage. 2016;141:242–9.

118. Zhou J, Heo HY, Knutsson L, van Zijl PCM, Jiang S. APT-weighted MRI: techniques, current neuro applications, and challenging issues. J Magn Reson Imaging. 2019;50(2):347–64.

119. Zhao X, Wen Z, Huang F, Lu S, Wang X, Hu S, et al. Saturation power dependence of amide proton transfer image contrasts in human brain tumors and strokes at 3 T. Magn Reson Med. 2011;66(4):1033–41.

120. Msayib Y, Harston GWJ, Tee YK, Sheerin F, Blockley NP, Okell TW, et al. Quantitative CEST imaging of amide proton transfer in acute ischaemic stroke. Neuroimage Clin. 2019;23:101833.

121. Lin G, Zhuang C, Shen Z, Xiao G, Chen Y, Shen Y, et al. APT weighted MRI as an effective imaging protocol to predict clinical outcome after acute ischemic stroke. Front Neurol. 2018;9:901.

122. Wang M, Hong X, Chang CF, Li Q, Ma B, Zhang H, et al. Simultaneous detection and separation of hyperacute intracerebral hemorrhage and cerebral ischemia using amide proton transfer MRI. Magn Reson Med. 2015;74(1):42–50.

123. Zheng S, van der Bom IM, Zu Z, Lin G, Zhao Y, Gounis MJ. Chemical exchange saturation transfer effect in blood. Magn Reson Med. 2014;71(3):1082–92.

124. Ma X, Bai Y, Lin Y, Hong X, Liu T, Ma L, et al. Amide proton transfer magnetic resonance imaging in detecting intracranial hemorrhage at different stages: a comparative study with susceptibility weighted imaging. Sci Rep. 2017;7:45696.

125. Anonymous. Global, regional, and national burden of Alzheimer's disease and other dementias, 1990-2016: a systematic analysis for the global burden of disease study 2016. Lancet Neurol. 2019;18(1):88–106.

126. Wells JA, O'Callaghan JM, Holmes HE, Powell NM, Johnson RA, Siow B, et al. In vivo imaging of tau pathology using multiparametric quantitative MRI. Neuroimage. 2015;111:369–78.

127. Wang R, Chen P, Shen Z, Lin G, Xiao G, Dai Z, et al. Brain amide proton transfer imaging of rat with Alzheimer's disease using saturation with frequency alternating RF irradiation method. Front Aging Neurosci. 2019;11:217.

128. Wang R, Wang C, Dai Z, Chen Y, Shen Z, Xiao G, et al. An amyloid-β targeting chemical exchange saturation transfer probe for in vivo detection of Alzheimer's disease. ACS Chem Neurosci. 2019;10(8):3859–67.

129. Chen L, Wei Z, Chan KWY, Cai S, Liu G, Lu H, et al. Protein aggregation linked to Alzheimer's disease revealed by saturation transfer MRI. NeuroImage. 2019;188:380–90.

130. Yang Y, Zhang J, Xiong L, Deng M, Wang J, Xin J, et al. Cognitive improvement induced by environment enrichment in chronic cerebral hypoperfusion rats: a result of upregulated endogenous neuroprotection? J Mol Neurosci. 2015;56(2):278–89.

131. Wang R, Li SY, Chen M, Zhou JY, Peng DT, Zhang C, et al. Amide proton transfer magnetic resonance imaging of Alzheimer's disease at 3.0 Tesla: a preliminary study. Chin Med J. 2015;128(5):615–9.

132. Cai K, Haris M, Singh A, Kogan F, Greenberg JH, Hariharan H, et al. Magnetic resonance imaging of glutamate. Nat Med. 2012;18(2):302–6.

133. Haris M, Nath K, Cai K, Singh A, Crescenzi R, Kogan F, et al. Imaging of glutamate neurotransmitter alterations in Alzheimer's disease. NMR Biomed. 2013;26(4):386–91.

134. Crescenzi R, DeBrosse C, Nanga RP, Reddy S, Haris M, Hariharan H, et al. In vivo measurement of glutamate loss is associated with synapse loss in a mouse model of tauopathy. NeuroImage. 2014;101:185–92.

135. Rupsingh R, Borrie M, Smith M, Wells JL, Bartha R. Reduced hippocampal glutamate in Alzheimer disease. Neurobiol Aging. 2011;32(5):802–10.

136. Antuono PG, Jones JL, Wang Y, Li SJ. Decreased glutamate + glutamine in Alzheimer's disease detected in vivo with (1)H-MRS at 0.5 T. Neurology. 2001;56(6):737–42.

137. Crescenzi R, DeBrosse C, Nanga RP, Byrne MD, Krishnamoorthy G, D'Aquilla K, et al. Longitudinal imaging reveals subhippocampal dynamics in glutamate levels associated with histopathologic events in a mouse model of tauopathy and healthy mice. Hippocampus. 2017;27(3):285–302.

138. Haris M, Singh A, Cai K, Nath K, Crescenzi R, Kogan F, et al. MICEST: a potential tool for non-invasive detection of molecular changes in Alzheimer's disease. J Neurosci Methods. 2013;212(1):87–93.

139. Yanez Lopez M, Pardon MC, Baiker K, Prior M, Yuchun D, Agostini A, et al. Myoinositol CEST signal in animals with increased Iba-1 levels in response to an inflammatory challenge-preliminary findings. PLoS One. 2019;14(2):e0212002.

140. Haris M, Cai K, Singh A, Hariharan H, Reddy R. In vivo mapping of brain myo-inositol. Neuroimage. 2011;54(3):2079–85.

141. Chen L, Wei Z, Chan KW, Li Y, Suchal K, Bi S, et al. D-glucose uptake and clearance in the tauopathy Alzheimer's disease mouse brain detected by on-resonance variable delay multiple pulse MRI. J Cereb Blood Flow Metab. 2020;41(5):1013–25.

142. Tolomeo D, Micotti E, Serra SC, Chappell M, Snellman A, Forloni G. Chemical exchange saturation transfer MRI shows low cerebral 2-deoxy-d-glucose uptake in a model of Alzheimer's disease. Sci Rep. 2018;8(1):9576.

143. Li C, Peng S, Wang R, Chen H, Su W, Zhao X, et al. Chemical exchange saturation transfer MR imaging of Parkinson's disease at 3 Tesla. Eur Radiol. 2014;24(10):2631–9.

144. Li C, Wang R, Chen H, Su W, Li S, Zhao X, et al. Chemical exchange saturation transfer MR imaging is superior to diffusion-tensor imaging in the diagnosis and severity evaluation of Parkinson's disease: a study on substantia nigra and striatum. Front Aging Neurosci. 2015;7:198.

145. Li C, Chen M, Zhao X, Wang R, Chen H, Su W, et al. Chemical exchange saturation transfer MRI signal loss of the substantia nigra as an imaging biomarker to evaluate the diagnosis and severity of Parkinson's disease. Front Neurosci. 2017;11:489.

146. Tong J, Wong H, Guttman M, Ang LC, Forno LS, Shimadzu M, et al. Brain alpha-synuclein accumulation in multiple system atrophy, Parkinson's disease and progressive supranuclear palsy: a comparative investigation. Brain. 2010;133(Pt 1):172–88.

147. Bagga P, Pickup S, Crescenzi R, Martinez D, Borthakur A, D'Aquilla K, et al. In vivo glucest MRI: reproducibility, background contribution and source of glutamate changes in the MPTP model of Parkinson's disease. Sci Rep. 2018;8(1):2883.

148. Bagga P, Crescenzi R, Krishnamoorthy G, Verma G, Nanga RP, Reddy D, et al. Mapping the alterations in glutamate with GluCEST MRI in a mouse model of dopamine deficiency. J Neurochem. 2016;139(3):432–9.

149. Anonymous. Global, regional, and national burden of multiple sclerosis 1990-2016: a systematic analysis for the global burden of disease study 2016. Lancet Neurol. 2019;18(3):269–85.

150. Rocca MA, Amato MP, De Stefano N, Enzinger C, Geurts JJ, Penner IK, et al. Clinical and imaging assessment of cognitive dysfunction in multiple sclerosis. Lancet Neurol. 2015;14(3):302–17.

151. Liu T, Chen Y, Thomas AM, Song X. Cest MRI with distribution-based analysis for assessment of early stage disease activity in a mouse model of multiple sclerosis: an initial study. NMR Biomed. 2019;32(11):e4139.

152. Thomas AM, Xu J, Calabresi PA, van Zijl PCM, Bulte JWM. Monitoring diffuse injury during disease progression in experimental autoimmune encephalomyelitis with on resonance variable delay multiple pulse (ONVDMP) CEST MRI. Neuroimage. 2020;204:116245.

153. Dula AN, Asche EM, Landman BA, Welch EB, Pawate S, Sriram S, et al. Development of chemical exchange saturation transfer at 7 T. Magn Reson Med. 2011;66(3):831–8.

154. O'Grady KP, Dula AN, Lyttle BD, Thompson LM, Conrad BN, Box BA, et al. Glutamate-sensitive imaging and evaluation of cognitive impairment in multiple sclerosis. Mult Scler. 2019;25(12):1580–92.

155. Ciccarelli O, Barkhof F, Bodini B, De Stefano N, Golay X, Nicolay K, et al. Pathogenesis of multiple sclerosis: insights from molecular and metabolic imaging. Lancet Neurol. 2014;13(8):807–22.

156. Dula AN, Pawate S, Dethrage LM, Conrad BN, Dewey BE, Barry RL, et al. Chemical exchange saturation transfer of the cervical spinal cord at 7 T. NMR Biomed. 2016;29(9):1249–57.

157. By S, Barry RL, Smith AK, Lyttle BD, Box BA, Bagnato FR, et al. Amide proton transfer CEST of the cervical spinal cord in multiple sclerosis patients at 3t. Magn Reson Med. 2018;79(2):806–14.

158. Hirtz D, Thurman D, Gwinn-Hardy K, Mohamed M, Chaudhuri A, Zalutsky RJN. How common are the "common" neurologic disorders? Neurology. 2007;68(5):326–37.

159. Thijs RD, Surges R, O'Brien TJ, Sander JW. Epilepsy in adults. Lancet. 2019;393(10172):689–701.

160. Duncan JS, Sander JW, Sisodiya SM, Walker MC. Adult epilepsy. Lancet. 2006;367(9516):1087–100.

161. Camacho DL, Castillo M. MR imaging of temporal lobe epilepsy. Semin Ultrasound CT MR. 2007;28(6):424–36.

162. Aitouche Y, Gibbs SA, Gilbert G, Boucher O, Bouthillier A, Nguyen DK. Proton MR spectroscopy in patients with nonlesional insular cortex epilepsy confirmed by invasive EEG recordings. J Neuroimaging. 2017;27(5):517–23.

163. O'Brien TJ, So EL, Mullan BP, Hauser MF, Brinkmann BH, Bohnen NI, et al. Subtraction ictal SPECT co-registered to MRI improves clinical usefulness of SPECT in localizing the surgical seizure focus. Neurology. 1998;50(2):445–54.

164. la Fougère C, Rominger A, Förster S, Geisler J, Bartenstein P. PET and SPECT in epilepsy: a critical review. Epilepsy Behav. 2009;15(1):50–5.

165. Burgess RC. Magnetoencephalography for localizing and characterizing the epileptic focus. Handb Clin Neurol. 2019;160:203–14.

166. Bradford HF. Glutamate, GABA and epilepsy. Prog Neurobiol. 1995;47(6):477–511.

167. Çavuş I, Romanyshyn JC, Kennard JT, Farooque P, Williamson A, Eid T, et al. Elevated basal glutamate and unchanged glutamine and GABA in refractory epilepsy: microdialysis study of 79 patients at the Yale epilepsy surgery program. Ann Neurol. 2016;80(1):35–45.

168. Davis KA, Nanga RP, Das S, Chen SH, Hadar PN, Pollard JR, et al. Glutamate imaging (GluCEST) lateralizes epileptic foci in nonlesional temporal lobe epilepsy. Sci Transl Med. 2015;7(309):309ra161.

169. Neal A, Moffat BA, Stein JM, Nanga RPR, Desmond P, Shinohara RT, et al. Glutamate weighted imaging contrast in gliomas with 7 Tesla magnetic resonance imaging. Neuroimage Clin. 2019;22:101694.

170. Kumar R. Understanding and managing acute encephalitis. F1000Research. 2020;9.

171. Jia Y, Chen Y, Geng K, Cheng Y, Li Y, Qiu J, et al. Glutamate chemical exchange saturation transfer (GluCEST) magnetic resonance imaging in pre-clinical and clinical applications for encephalitis. Front Neurosci. 2020;14:750.

172. Zhang Z, Bassam B, Thomas AG, Williams M, Liu J, Nance E, et al. Maternal inflammation leads to impaired glutamate homeostasis and up-regulation of glutamate carboxypeptidase II in activated microglia in the fetal/newborn rabbit brain. Neurobiol Dis. 2016;94:116–28.